# An Alternative Clamp Loading Pathway via the T4 Clamp Loader gp44/62−DNA Complex†

Zhihao Zhuang,‡ Anthony J. Berdis,§ and Stephen J. Benkovic*,‡

*Department of Chemistry, 414 Wartik Laboratory, The Pennsylvania State University, University Park, Pennsylvania 16802, and Departments of Pharmacology and Chemistry, Case Western Reserve University, 10900 Euclid Avenue, Cleveland, Ohio 44106*

*Received January 19, 2006; Revised Manuscript Received April 17, 2006*

ABSTRACT: In bacteriophage T4, a clamp loading pathway that utilizes the T4 clamp loader (gp44/62) and ATP hydrolysis initially to form a complex with the clamp (gp45) has been demonstrated, followed by interaction with DNA and closing of the clamp. However, the recent observation that gp45 exists as an opened form in solution raises the possibility of other pathways for clamp loading. In this study, an alternative clamp loading sequence is evaluated in which gp44/62 first recognizes the DNA substrate and then sequesters the clamp from solution and loads it onto DNA. This pathway differs in terms of the initial formation of a gp44/62−DNA complex that is capable of loading gp45. In this work, we demonstrate ATP-dependent DNA binding by gp44/62. Among various DNA structures that were tested, gp44/62 binds specifically to primer−template DNA but not to single-stranded DNA or blunt-end duplex DNA. By tracing the dynamic clamp closing with pre-steady-state FRET measurements, we show that the clamp loader−DNA complex is functional in clamp loading. Furthermore, pre-steady-state ATP hydrolysis experiments suggest that 1 equiv of ATP is hydrolyzed when gp44/62 binds to DNA, and additional ATP hydrolysis is associated with the completion of the clamp loading process. We also investigated the detailed kinetics of binding of MANT-nucleotide to gp44/62 through stopped-flow FRET and demonstrated a conformational change as the result of ATP, but not ADP binding. The collective kinetic data allowed us to propose and evaluate a sequence of steps describing this alternative pathway for clamp loading and holoenzyme formation.

The T4 replisome is responsible for accurate and processive synthesis of the bacteriophage genomic DNA. The T4 DNA polymerase (gp43) constitutes the core of the replisome and is able to synthesize complementary DNA in a 5′-to-3′ direction (*1*, *2*). The polymerase alone is not processive; i.e., it produces short DNA product strands (<10 nucleotides) per binding event (*3*), which is insufficient for continuous replication of the T4 genomic DNA (∼170 kb). The same dilemma is faced by other prokaryotic and eukaryotic replicative polymerases, including *Escherichia coli* Pol III and yeast Pol $\delta$ (*4*). In the T4 replisome, another essential protein component, gp45, acts to enhance the processivity of the polymerase by topologically tethering it to DNA. gp45 is a homotrimeric protein with a toroidal shape that encircles duplex DNA and allows the sliding of gp45 on DNA. The polymerase gp43 is physically linked to gp45 through the interaction between its C-terminus and the clamp (*5*). In an ATP-dependent process, a clamp loader protein gp44/62 acts as a catalytic "matchmaker" to properly position, orient, and load the clamp on DNA. Similar strategies are used by other prokaryotic and eukaryotic replication systems. The $\beta$ subunit and $\gamma$ complex in *E. coli* as well as the proliferating cell nuclear antigen (PCNA) and RFC complex in *Saccharomyces cerevisiae* are functionally homologous to T4 clamp gp45 and clamp loader gp44/62.

Previous mechanistic studies of the clamp loading process from bacteriophage T4 and *E. coli* have outlined the molecular events in clamp loading and holoenzyme formation (*6*−*9*). Although some common mechanistic characteristics are shared by the two systems, there are specific differences. One unique difference is with respect to the stoichiometry and timing of ATP hydrolysis by the two clamp loaders. In the T4 system, two of the four ATPs bound by gp44/62 (the clamp loader is tetrameric in gp44 and monomeric in gp62) undergo hydrolysis upon interaction with gp45 to form the clamp−clamp loader complex. Two additional ATPs are presumably hydrolyzed once the same complex encounters DNA to complete loading of the clamp onto duplex DNA. In *E. coli*, however, ATP binding rather than hydrolysis provides the driving force for clamp opening (*10*). Hydrolysis of two or three ATPs bound by the $\gamma$ complex can effectively close the clamp and dissociate the clamp loader from DNA (*9*).

The high-resolution X-ray crystal structures of the clamps from bacteriophage T4 (gp45), *E. coli* ($\beta$ subunit), and *S. cerevisiae* (PCNA) demonstrated structural similarities despite the low level of sequence identity among them. In the crystal structures, all three clamp proteins form closed rings using either three (gp45 and PCNA) or two ($\beta$ subunit) identical subunits. However, in solution, T4 clamp gp45 is

† This work was supported by National Institutes of Health Grant GM13306 to S.J.B.

* To whom correspondence should be addressed. E-mail: sjb1@psu.edu. Phone: (814) 865-2882. Fax: (814) 865-2973.

‡ The Pennsylvania State University.

§ Case Western Reserve University.

10.1021/bi0601205 CCC: $33.50 
Published on Web 06/07/2006

open at one subunit interface with a separation distance of 42 Å, while closed at the other two interfaces (17 Å) (*11*, *12*). Moreover, the T4 clamp is much less stable, dissociating into subunits with a $K_d$ of 250 nM compared to the dissociation of PCNA and $\beta$ subunit ($K_d \sim 21$ nM and $K_d <$ 60 pM, respectively) (*13*). This difference in clamp stability is commensurate with the strength of subunit interactions as revealed by crystal structures (*14*).

The confirmation of a static open form of gp45 in solution by time-resolved FRET[1] measurements (*12*) raised an intriguing question regarding the role of gp44/62 in clamp loading and the need for ATP hydrolysis. Since gp45 is open in solution with an interface distance separation large enough to allow the passage of dsDNA, why is the clamp loader (gp44/62) needed presumably to further open the clamp with the consumption of two ATPs in the rapid initial steps of clamp loading onto DNA? In this study, we address this question by seeking an alternative way of clamp loading in forming the holoenzyme. Specifically, we tested the hypothesis that gp44/62 might function to initially mark the locus of clamp loading by binding at the 3′-end of primed DNA followed by sequestering and loading of the clamp protein. The clamp loader was found to avidly bind to primer−template DNA in the presence of ATP but in the absence of gp45 through surface plasmon resonance (SPR) studies. The stoichiometry of rapid ATP hydrolysis by gp44/62 measured by fast kinetic methods for this pathway was reduced to 1 equiv of ATP consumption. The ability of this gp44/62−DNA complex to load the clamp onto DNA was assessed by tracking changes in distance across the gp45 subunit interface through a Trp−CPM [7-diethylamino-3-(4′-maleimidylphenyl)-4-methylcoumarin] FRET probe at the subunit interface. This clamp loading sequence, which takes advantage of the opened clamp protein, is compared to its counterparts in the *E. coli* and yeast DNA replication systems.

## MATERIALS AND METHODS

Oligonucleotide primers and substrates were prepared as previously described (*15*). The forked Bio62/34/36mer primer−template forked DNA blocked with streptavidin was used in the stopped-flow and rapid quench experiments. 7-Diethylamino-3-(4′-maleimidylphenyl)-4-methylcoumarin (CPM) and streptavidin were obtained from Molecular Probes (Eugene, OR). ATP and ATP$\gamma$S were obtained from Roche Molecular Biochemicals (Indianapolis, IN). [$\gamma$-$^{32}$P]ATP was purchased from PerkinElmer. All other materials were obtained from commercial sources and were of the highest available quality. The assay buffer used in all kinetic experiments consisted of 25 mM Tris-OAc (pH 7.5), 125 mM KOAc, and 5 mM MgOAc. T4 proteins exo$^-$ gp43, gp45, and gp44/62 were prepared as previously described (*16*, *17*). Clamp loader mutant gp44(K56A)/62 was purified the same way as wild-type gp44/62. The gp44 subunit was purified by following the published procedure (*18*). The purification of double mutant gp45 (V163C/W199F) and triple mutant gp45 (W92F/V163C/W199F) and their labeling with CPM were performed as previously reported (*11*).

[1] Abbreviations: CPM, 7-diethylamino-3-(4′-maleimidylphenyl)-4-methylcoumarin; FRET, fluorescence resonance energy transfer; MANT-ATP, 2′- and 3′-*O*-(*N*-methylanthraniloyl)ATP; MANT-ADP, 2′- and 3′-*O*-(*N*-methylanthraniloyl)ADP; SPR, surface plasmon resonance.

*MANT-Nucleotide Binding Probed by Stopped-Flow FRET.* Transient kinetic measurements of the extent of binding of MANT-nucleotide to gp44/62 were taken using an Applied Photophysics (Leatherhead, Surrey, U.K.) SX.18MV stopped-flow reaction analyzer in fluorescence mode thermostated at a constant temperature of 25 °C. The mixer has a dead time of 1.7 ms. The excitation wavelength was set at 290 nm, and the MANT fluorescence was detected using a 450 nm cutoff filter. Nonlinear least-squares fitting was carried out using the software provided with the instrument. The concentrations stated herein are the final concentrations after mixing.

To measure the kinetics of binding of MANT-nucleotide to gp44/62, 250 nM gp44/62 was mixed with either MANT-ATP or MANT-ADP at concentrations varying from 2.5 to 80 $\mu$M. The data traces showing a MANT fluorescence increase were fitted to equations that describe either a single exponential (eq 1) or a double exponential (eq 2) using the software provided to obtain an observed rate constant ($k_{obs}$).

$$F = A \exp(-k_{obs}t) + C \quad (1)$$

$$F = A_1 \exp(-k_{obs,1}t) + A_2 \exp(-k_{obs,2}t) + C \quad (2)$$

where $F$ is the fluorescence intensity in arbitrary units, $A$ is the amplitude of the curve in terms of fluorescence intensity, $C$ is the fluorescence intensity at infinite time, and $k_{obs}$ is the observed rate constant (inverse seconds).

The binding of MANT-nucleotide to clamp loader subunit gp44 was studied in the same way except that 2.5 $\mu$M gp44 was used. To directly measure the kinetics of dissociation of bound MANT-ATP and MANT-ADP from gp44/62 or gp44, 250 nM gp44/62 or 2.5 $\mu$M gp44, respectively, was preincubated with 20 $\mu$M MANT-nucleotide for 10 min at room temperature and then rapidly mixed with a solution that contains an excess of ATP (1 mM) and an equal amount of MANT-nucleotide (20 $\mu$M). The inclusion of an equal concentration of MANT-nucleotide in both syringes prevents the dissociation of MANT-nucleotide due to a dilution effect. The kinetics of dissociation of MANT-nucleotide from gp44/62 or gp44 were determined by fitting the fluorescence trace to a single-exponential equation to obtain the dissociation rate constant.

*Surface Plasmon Resonance Biosensor Measurements.* The real-time surface plasmon resonance (SPR) binding measurements were performed on the BIAcore 2000 system (Biacore, Uppsala, Sweden) using Biacore SA chips, which contain carboxymethylated dextran preimmobilized with streptavidin for immobilization of biotinylated interaction partners. The running buffer used for analysis contains 10 mM Tris (pH 7.5), 150 mM NaCl, 5 mM $MgCl_2$, and 0.005% P20 detergent (Biacore Inc., Piscataway, NJ). All buffer solutions were freshly prepared, degassed, and passed through a 0.22 $\mu$m pore size filter. All experiments were carried out at 25 °C. The DNA ligands used for binding studies include a single-stranded DNA 30mer with a 5′-biotin (Bio30mer; see Table 1 for DNA oligo sequences), a primer−template DNA (P−T DNA) with a recessed 3′-end formed by annealing a 60mer DNA oligo to the Bio30mer, and a blunt-end duplex DNA formed by annealing a 30mer DNA oligo to the Bio30mer. Special care was taken in the design of the DNA sequence to prevent complications from potential DNA secondary

Table 1: Sequences of DNA Ligands Used for SPR Measurements

| | |
|---|---|
| Single-stranded DNA | |
| | 5′ Bio-AGGGAAGGGAGAGGGAGGAGAAGAAGGGAG 3′ |
| Blunt-end duplex DNA | |
| | 5′ Bio-AGGGAAGGGAGAGGGAGGAGAAGAAGGGAG 3′ |
| | TCCCTTCCCTCTCCCTCCTCTTCTTCCCTC |
| Primer-Template DNA | |
| | 5′ Bio-AGGGAAGGGAGAGGGAGGAGAAGAAGGGAG 3′ |
| | $TCCCTTCCCTCTCCCTCCTCTTCTTCCCTCT_{30}$ |

structures in the single-stranded DNA region. The DNA ligands were immobilized on the sensor chip through biotin−streptavidin interactions by controlled injection of DNA ligands diluted in 10 mM Tris (pH 7.5), 1.2 M NaCl, and 0.005% P20 solution onto the chip surface at a constant flow rate of 10 $\mu$L/min. The charged sensor surface was then washed with running buffer to remove nonspecifically bound DNA oligos until a stable baseline was obtained. For qualitative binding analysis, approximately 200 response units (RU) of DNA oligos was immobilized onto the sensor chip surface. To correct for nonspecific binding and bulk refractive index changes, a blank flow cell on the sensor chip without DNA oligos was used as a control. The difference in RU between the DNA charged flow cell and the control flow cell represents the true binding signal. In a typical run, T4 clamp loader gp44/62 or its subunit gp44 was injected into the flow cell either alone or in the presence of different nucleotides, including ATP (1 mM), ADP (1 mM), or ATP$\gamma$S (1 mM). The experiments were carried out in parallel with sensor chips charged with either single-stranded DNA, P−T DNA with a 3′-recessed end, or a blunt-end duplex DNA, respectively. The real-time response unit changes for the association and dissociation phases were recorded.

To obtain kinetic information for binding of gp44/62 to P−T DNA, approximately 10 RU of DNA oligo was immobilized on a sensor chip. Fifty microliters of sample solutions that contain gp44/62 at various concentrations (up to 400 nM) and 1 mM ATP were injected over the DNA-modified sensor surface for 2.5 min at a constant flow rate of 20 $\mu$L/min, followed by washing with running buffer for 5 min. The sensorgrams for both association and dissociation phases were recorded in real time. For kinetic analysis, the sensorgrams were despiked and corrected for bulk refractive index changes to generate data amenable for analysis.

The binding and dissociation data were analyzed using CLAMP (version 99). Several models, including a simple 1:1 Langmuir binding model, a surface heterogeneity model, a Langmuir model with the mass transfer effect, and a simple conformation change model, were surveyed to fit the data. However, none of these simple models can adequately fit the data. On the basis of the fact that DNA binding can trigger the ATP hydrolysis by gp44/62, a three-step reaction mechanism involving an intermediate species (ED*) as described in Scheme 1 was used to fit the data.

E represents gp44/62, and D represents P−T DNA. ED stands for the gp44/62−DNA complex, and ED* stands for an intermediate specie converted from ED. The data were globally analyzed by fitting both the association and dissociation phases for several gp44/62 concentrations. The degree of randomness of residual plots was used to determine the goodness of the fit.

Scheme 1

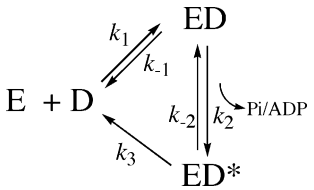


*Stopped-Flow Fluorescence Spectroscopy.* Stopped-flow fluorescence experiments were performed on an Applied Photophysics SX.18MV stopped-flow reaction analyzer in fluorescence mode at a constant temperature of 25 °C. The samples were excited at 290 nm for gp45 double mutant V163C/W199F-CPM and at 290 and 390 nm for gp45 triple mutant W92F/V163C/W199F-CPM. A 420 nm cutoff filter was used to detect the CPM fluorescence. When samples were excited at 290 nm and detected above 420 nm, the fluorescence signals include both intraprotein and interprotein FRET between tryptophan(s) (in either gp45 or gp44/62) and the gp45 V163C-CPM fluorophore, as well as the fluorescence signal from direct excitation of CPM. By exciting the fluorophore at 390 nm, we detected fluorescence from direct CPM excitation exclusively. The fluorescence signal was normalized as reported in a previous study (*6*). The normalized fluorescence changes of exciting the gp45 double mutant ($F_{AD}^{290}$) were corrected for changes in fluorophore environment ($F_A^{390}$) and interprotein FRET ($F_A^{290}$) and converted to fluorescence intensity ($I_{AD}$ and $I_A$) as described previously (*6*).

The W92−V163C-CPM distances were obtained using the following equations that calculate the energy transfer efficiency and averaged distance based on acceptor sensitization.

$$E_T = \left(\frac{I_{AD}}{I_A} - 1\right)\frac{\epsilon_A}{\epsilon_D} \quad (3)$$

$$R = R_0\left(\frac{1}{E_T} - 1\right)^{1/6} \quad (4)$$

where $E_T$ is the energy transfer efficiency at all three subunit interfaces, $I_{AD}$ and $I_A$ are the fluorescence intensities of the CPM acceptor in the presence and absence, respectively, of the tryptophan donor at the donor excitation wavelength of 290 nm, $\epsilon_A$ and $\epsilon_D$ are the extinction coefficients of the CPM acceptor and Trp donor, respectively, at 290 nm (previously determined to be 3340 and 4100 $M^{-1}$ $cm^{-1}$, respectively), $R_0$ is the Forster distance at which the transfer efficiency is 50% (previously determined to be 31 Å), and $R$ is the distance between the donor and acceptor.

The experimentally determined FRET energy transfer efficiency ($E_T$) is the averaged distances between W92 and V163C-CPM at all three subunit interfaces. The following equation (eq 5) was used to calculate the energy transfer efficiency for the opened subunit interface ($E_O$)

$$E_O = 3E_T - 2E_C \quad (5)$$

based on the assumption that two of the three subunit

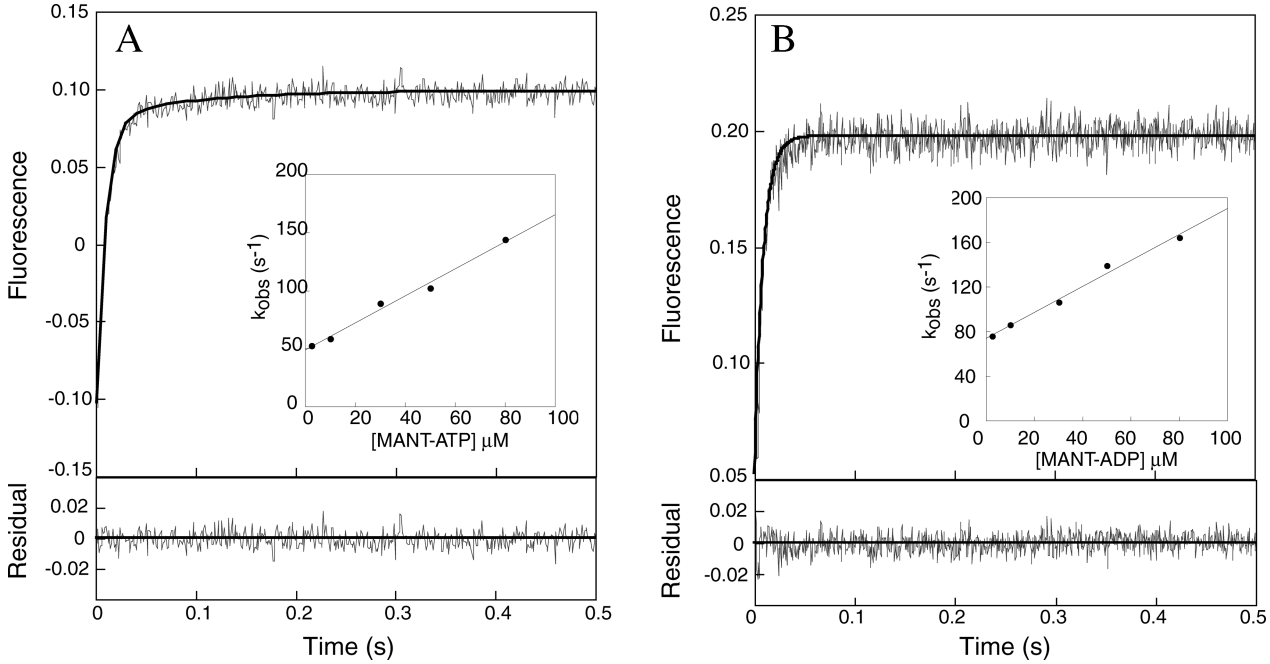


FIGURE 1: Representative stopped-flow fluorescence trace measuring the level of binding of nucleotide analogue MANT-ATP (A) and MANT-ADP (B) to gp44/62. The inset shows the concentration dependence of the $k_{obs,1}$ of binding of MANT-ATP (A) and MANT-ADP (B) to gp44/62. The fluorescence signal of binding of MANT-nucleotide to gp44/62 was fitted to either a single- or double-exponential equation (residuals shown) to obtain the observed rate constants (see Results). The rate constant of the binding phase was plotted vs MANT-nucleotide concentration, and the plot was fitted to the equation $k_{obs} = k_{on}$[MANT-nucleotide] + $k_{off}$ by linear regression using KaleidaGraph.

interfaces are closed with an energy transfer efficiency ($E_C$) of 0.95 (*6*). Therefore, the distance between donor and acceptor probes can be calculated which in turn reflects the separation between subunits of an open interface.

*Pre-Steady-State ATP Hydrolysis Measurements.* All assays monitoring the hydrolysis of [$\gamma$-$^{32}$P]ATP by gp44/62 were performed as previously described (*7*). Pre-steady-state ATPase measurements were performed using a rapid quench instrument. At various time intervals ($\Delta t = 0.01-5$ s), the reaction was quenched through the addition of 1 M hydrochloric acid. The samples were then extracted with 100 $\mu$L of a phenol/chloroform mixture and then neutralized by the addition of approximately 35 $\mu$L of 3 M NaOH and 1 M Tris. Samples were analyzed using thin-layer chromatography to separate $^{32}P_i$ from nonhydrolyzed [$\gamma$-$^{32}$P]ATP using PEI-F cellulose TLC plates developed with 0.6 M potassium phosphate buffer (pH 3.5). TLC images were obtained with a Molecular Dynamics PhosphorImager. Product formation was quantified by measuring the ratio of $^{32}P_i$ product to unhydrolyzed [$\gamma$-$^{32}$P]ATP substrate. The ratios of product formation are corrected for substrate hydrolysis in the absence of enzyme (zero point). Corrected ratios are then multiplied by the final concentration of ATP (250 $\mu$M) used in each assay to yield the total concentration of ATP hydrolyzed.

## RESULTS

*Binding of Adenosine Nucleotide to Clamp Loader gp44/62 or Subunit gp44 Probed with Stopped-Flow Fluorescence Spectroscopy.* The kinetic parameters for ATP hydrolysis catalyzed by gp44/62 have been reported by several groups (*19*−*21*). However, the kinetic events associated with binding of the nucleotide to the clamp loader protein have not been elucidated. To this end, we used stopped-flow fluorescence spectroscopy to probe the kinetics of binding of nucleotide analogues MANT-ATP and MANT-ADP to gp44/62 or its subunit, gp44. The fluorescent nucleotide analogues MANT-ATP and MANT-ADP have been successfully used to probe the binding of nucleotide to numerous ATP-utilizing proteins, including *E. coli* Rep helicase (*22*), myosin (*23*), and tyrosine kinase (*24*). Although changes in fluorescence were observed when MANT-ATP and MANT-ADP bound to gp44/62 (data not shown), the high background fluorescence signal of the MANT fluorophore makes it impractical to use the high concentrations needed to measure an accurate binding constant. To circumvent this complication, we assessed the fluorescence resonance energy transfer (FRET) between the excited protein tryptophan residues of gp44/62 (or gp44) and the MANT-nucleotide fluorophore. The time-dependent increases in MANT fluorescence observed at varied nucleotide (Nt) concentrations were measured, and the generated time courses were fit to either single- or double-exponential equations to determine the observed rate constant ($k_{obs}$) for each transient. A representative time course is provided in Figure 1A in which 50 $\mu$M MANT-ATP was mixed with 250 nM gp44/62. Comparing the fit of this transient to both single- and double-exponential equations showed that the latter yields a better fitting as judged by the randomness of residuals. Two phases can be observed in the transient of binding of MANT-ATP to gp44/62. The first fast phase occurs with an observed rate constant $k_{obs,1}$ of 106 ± 7 $s^{-1}$ and an amplitude $A_1$ of 0.20 and is followed by a slower phase of fluorescence increase ($k_{obs,2} = 15.2 \pm 3$ $s^{-1}$ and $A_2 = 0.021$). Biphasic time courses for the kinetics of binding of MANT-ATP to gp44/62 were observed using MANT-ATP concentrations from 2.5 to 80 $\mu$M. A linear correlation was found for the rate constant of the fast phase ($k_{obs,1}$) versus MANT-ATP concentration over the range of nucleotide

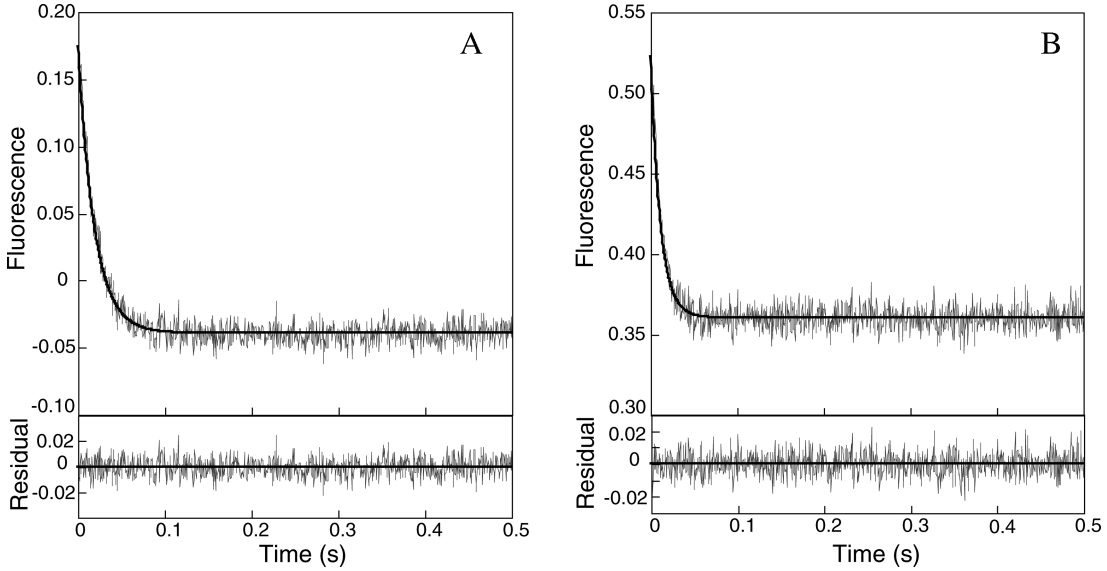


FIGURE 2: Representative stopped-flow fluorescence trace measuring the dissociation of MANT-ATP (A) and MANT-ADP (B) from gp44/62 via a nucleotide chasing experiment. gp44/62 (250 nM) was preincubated with 20 $\mu$M MANT-nucleotide and then rapidly mixed with a solution containing an excess of ATP (1 mM) and an equal amount of MANT-nucleotide (20 $\mu$M). The kinetics of dissociation of MANT-nucleotide from gp44/62 were determined by fitting the fluorescence trace to a single-exponential equation to obtain the dissociation rate constant.

analogue concentrations that were tested (Figure 1A, inset). The resulting data were fit according to a one-step binding mechanism (eq 6) to yield an apparent bimolecular association rate constant ($k_{on}$) of $1.16 \times 10^6$ $M^{-1}$ $s^{-1}$ and a dissociation rate constant of 49 $s^{-1}$. The second phase rate constant exhibited a nonlinear dependency on MANT-ATP concentration, suggesting this step is likely reversible. However, the scattering of the data prevented us from parsing $k_{obs,2}$ into microscopic rate constants.

$$k_{obs} = k_{on}[Nt] + k_{off} \quad (6)$$

A similar increase in MANT fluorescence was also observed upon binding of MANT-ADP to gp44/62. Unlike the case of binding of MANT-ATP to gp44/62, these data can be satisfactorily fitted to a single-exponential equation (Figure 1B). The observed rate constant, $k_{obs}$, increased linearly as the concentration of MANT-ADP was increased from 2.5 to 80 $\mu$M (Figure 1B, inset). Fitting the data to eq 6 yielded a bimolecular association rate constant $k_{on}$ of $1.16 \times 10^6$ $M^{-1}$ $s^{-1}$ and a MANT-ADP dissociation rate constant of 74 $s^{-1}$.

The kinetics of dissociation of MANT-ATP and MANT-ADP from gp44/62 were also examined by preincubating 250 nM gp44/62 with either 20 $\mu$M MANT-ATP or 20 $\mu$M MANT-ADP and then rapidly chasing with an excess of ATP (1 mM). In both cases, a single-exponential decrease in the magnitude of the fluorescence signal was observed (Figure 2) that reflects dissociation of the MANT-nucleotide. The dissociation rate constants of MANT-nucleotide from gp44/62 active sites were determined by fitting the traces to the single-exponential equation. The dissociation rate constant ($k_{off}$) of MANT-ATP was determined to be 53 $s^{-1}$ and was not affected by ATP concentrations greater than 1 mM. Similarly, a rate constant of 89 $s^{-1}$ was obtained for dissociation of MANT-ADP from gp44/62. In general, the dissociation rate constants determined directly from the chase experiments are more accurate than the values (although in satisfactory agreement) determined by extrapolating the straight line of $k_{obs} \sim$ [MANT-nucleotide] as described above. Therefore, the rate constants determined from chase experiments were used to calculate the equilibrium dissociation constants, $K_d$ (see Table 1). The calculated $K_d$ of 46 $\mu$M for binding of MANT-ATP to gp44/62 is close to the previously reported value of 34 $\mu$M determined by an equilibrium binding experiment using [$\gamma$-$^{32}$P]ATP (*25*). However, the $K_d$ of 77 $\mu$M measured for MANT-ADP binding is 4.5-fold higher than the value of 17 $\mu$M determined in the same equilibrium binding experiment (*25*).

*Binding of MANT-Nucleotide to Clamp Loader Subunit gp44.* The ATP-binding site of the gp44/62 clamp loader protein resides solely on the gp44 subunit and not on the gp62 subunit (*26*). However, binding of nucleotide to the gp44 subunit in the absence of gp62 had not been characterized quantitatively. To evaluate the influence of the gp62 subunit on nucleotide binding, the kinetics of binding of MANT-nucleotide analogues to gp44 were also determined using stopped-flow FRET. For example, a double-exponential increase in the magnitude of the fluorescence signal was observed when 2.5 $\mu$M gp44 was mixed with 2.5−50 $\mu$M MANT-ATP (see the Supporting Information). The rate constants of the fast phase, $k_{obs,1}$, were plotted against varying MANT-ATP concentrations to obtain the bimolecular rate constant ($k_{on} = 1.93 \times 10^6$ $M^{-1}$ $s^{-1}$) and the dissociation rate constant ($k_{off} = 93$ $s^{-1}$) (see the Supporting Information). The dissociation rate constant of 84 $s^{-1}$ for MANT-ATP measured by the nucleotide chase protocol is in good agreement. In a similar way, the kinetic rate constant for binding of MANT-ADP to gp44 was determined to be $1.71 \times 10^6$ $M^{-1}$ $s^{-1}$ ($k_{on}$) with a dissociation rate constant of 84 $s^{-1}$ ($k_{off}$), in good agreement with the $k_{off}$ value of 88 $s^{-1}$ measured by the nucleotide chase protocol. The equilibrium rate constants, $K_d$, calculated from the measured $k_{on}$ and $k_{off}$ values are listed in Table 2.

*Binding of Clamp Loader gp44/62 to DNA Studied by Surface Plasmon Resonance.* The specificity of binding of

Table 2: Summary of Rate Constants Determined with Stopped-Flow FRET Experiments

| protein | nucleotide | $k_{on}$ ($M^{-1}$ $s^{-1}$) | $k_{off}$ ($s^{-1}$) | $k_{off}$ ($s^{-1}$)[a] | $K_d$ ($\mu$M) |
|---|---|---|---|---|---|
| gp44/62 | MANT-ATP | $(1.16 \pm 0.07) \times 10^6$ | $49 \pm 3$ | $53.4 \pm 0.9$ | $46 \pm 3$ |
| | MANT-ADP | $(1.16 \pm 0.07) \times 10^6$ | $74 \pm 3$ | $89 \pm 2$ | $77 \pm 6$ |
| gp44 | MANT-ATP | $(1.93 \pm 0.05) \times 10^6$ | $93 \pm 1$ | $84 \pm 1$ | $44 \pm 2$ |
| | MANT-ADP | $(1.71 \pm 0.06) \times 10^6$ | $84 \pm 1$ | $87.9 \pm 0.4$ | $52 \pm 2$ |

[a] Rate constant measured directly from competition experiments.

gp44/62 to DNA was investigated in detail using the surface plasmon resonance (SPR) technique that allows the detection of real-time binding of an analyte to the ligand immobilized on a sensor chip. In our studies, a streptavidin-coated sensor chip was used to immobilize the biotinylated DNA ligand. Three different DNA ligands were tested that include single-stranded DNA, blunt-end duplex DNA, and primer−template DNA (P−T DNA) containing a recessed 3′-end (see Table 1 for DNA sequences). Binding of gp44/62 to all three forms of oligonucleotides was monitored in the presence of 1 mM ATP (Figure 3A). gp44/62 was only capable of binding the primer−template DNA containing a recessed 3′-end. No significant binding to either single-stranded DNA or blunt-end duplex DNA was observed for gp44/62. These data indicate that gp44/62 possesses an intrinsic affinity for the defined structure present in the primer−template DNA end.

No significant binding of gp44/62 to P−T DNA was detected in the absence of ATP under identical experimental conditions (Figure 3B). These data suggest that binding of protein to DNA is dependent upon nucleotide binding and/or hydrolysis. To further investigate this hypothesis, we measured the effects of ATP$\gamma$S and ADP on binding since it was shown previously that both ATP$\gamma$S and ADP retain an affinity for gp44/62 similar to that of ATP (*19*). Interestingly, neither ATP$\gamma$S nor ADP can support binding of gp44/62 to the same P−T DNA (Figure 3B). Furthermore, when a competition experiment was carried out by including equal amounts of ATP and ATP$\gamma$S with gp44/62 in the SPR binding experiment, the extent of binding of gp44/62 to DNA was markedly reduced as detected by an approximately 4-fold decrease in the maximum resonance units (see the Supporting Information). This result suggests that ATP$\gamma$S indeed binds to the clamp loader protein; however, it does not support binding of gp44/62 to DNA. In a related experiment when ADP was used as a nucleotide competitor, a similar decrease in the level of gp44/62 binding was observed when equal amounts of ADP and ATP were included in the solution (data not shown).

Mutant clamp loader protein gp44(K56A)/62 was then used to further examine whether ATP hydrolysis is required for binding of gp44/62 to P−T DNA. Previous studies had shown that gp44(K56A)/62 loses its ATPase activities due to a mutation in the critical p-loop lysine residue but retains normal ATP and clamp protein gp45 binding ability (*27*). Mutant clamp loader protein gp44(K56A)/62 alone did not bind to P−T DNA as judged from the negligible resonance unit increase. No significant binding was observed, as expected, even in the presence of 1 mM ATP, ATP$\gamma$S, or ADP (Supporting Information).

*Clamp Loader Protein Subunit gp44 Retains DNA Binding Ability.* At present, the detailed information regarding how gp44/62 binds DNA is still very limited. It has been suggested that the gp44 subunits make close contact with DNA through cross-linking experiments (*28*). The contribution of subunit gp62 to productive DNA binding is not clear.

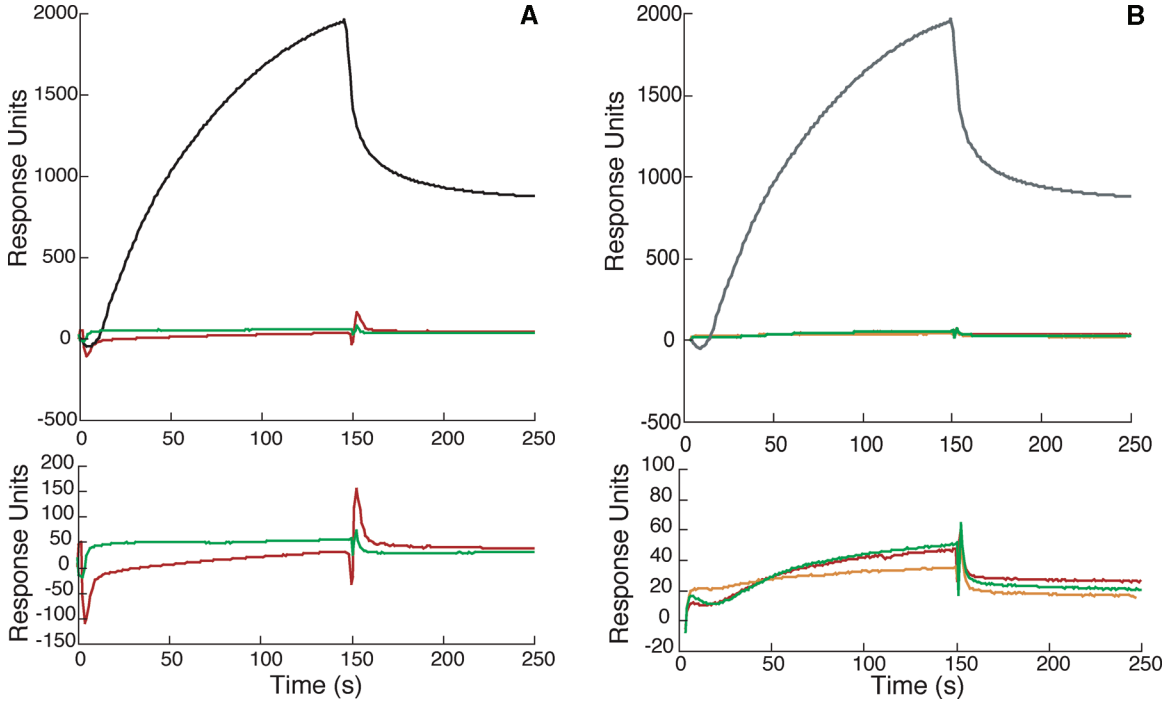


FIGURE 3: (A) SPR sensorgrams of binding of gp44/62 to P−T DNA (black), single-stranded DNA (red), and blunt-end duplex DNA (green) in the presence of 1 mM ATP. Approximately 200 RU of P−T DNA, single-stranded DNA, or blunt-end duplex DNA was immobilized on the SA chip surface through a 3′-end biotin−streptavidin interaction. The gp44/62 solution (200 nM) was injected at a flow rate of 20 $\mu$L/min in the presence of 1 mM ATP. The response unit represents the difference in response between the DNA charged flow cell and the blank control flow cell. The bottom panel is a close-up of the low response traces. (B) SPR sensorgram of binding of gp44/62 to P−T DNA in the absence of nucleotide (red) or in the presence of 1 mM ATP (black), ADP (green), and ATP$\gamma$S (orange). The bottom panel is a close-up of the low response traces.

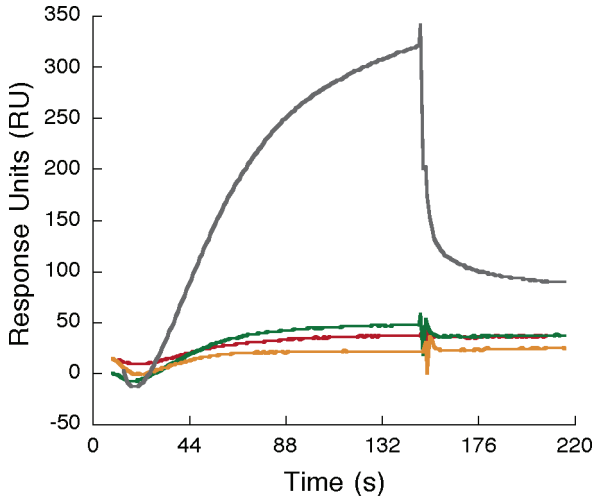


FIGURE 4: SPR sensorgram of binding of 200 nM gp44 subunit to P−T DNA in the absence of nucleotide (red) or in the presence 1 mM ATP (black), ADP (green), and ATP$\gamma$S (orange).

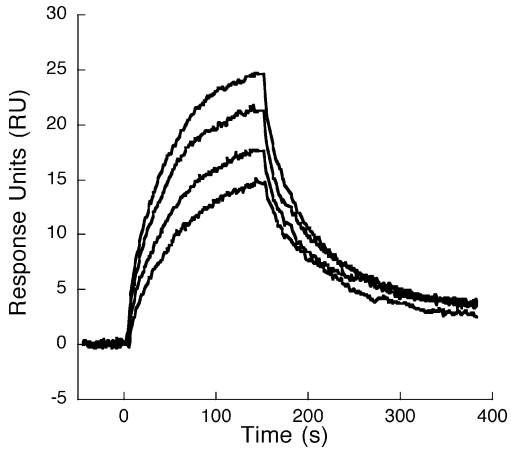


FIGURE 5: Sensorgrams of binding of gp44/62 to P−T DNA at increasing gp44/62 concentrations. Approximately 10 RU of P−T DNA was immobilized onto the chip surface. The gp44/62 concentrations that were tested were 200, 250, 300, and 400 nM, and 1 mM ATP was included in all experiments.

Here we tested whether the gp44 subunit retains P−T DNA binding ability and how this binding compares to that of the complete gp44/62 complex. SPR binding experiments demonstrated that the gp44 subunit indeed retains DNA binding ability provided that ATP is included (Figure 4). The resonance unit increase at the same protein molar concentration was smaller for gp44 than for the entire gp44/62 complex. This can be understood in light of the lower molecular weight of the gp44 subunit [gp44, however, may exist as a tetramer (Z. Zhuang, unpublished results)] or a reduced affinity of the gp44 subunit for DNA. The binding of gp44 to primer−template DNA is also strictly dependent upon ATP since neither ATP$\gamma$S nor ADP can support its binding to primer−template DNA (Figure 4). Furthermore, the gp44 subunit does not bind to single-stranded DNA or duplex DNA with a blunt end. Collectively, these data indicate that the gp44 subunit retains DNA binding capabilities as shown for the complete gp44/62 complex. This suggests, but does not prove, that the function of the gp62 subunit is to interact with the clamp protein and/or DNA polymerase during holoenzyme formation.

*Kinetics of Binding of Clamp Loader gp44/62 to DNA.* To obtain quantitative information about binding of gp44/62 to P−T DNA in the presence of ATP, a low level of P−T DNA (~10 resonance units) was bound to the Biacore SA chip. At a fixed concentration of ATP (1 mM), the real-time binding and dissociation of gp44/62 to and from P−T DNA immobilized on the sensor chip were followed at several different concentrations of gp44/62 (up to 400 nM). As shown in Figure 5, the number of overall sensor response units (RU) increases with higher concentrations of gp44/62 and validates binding of gp44/62 to the immobilized DNA.

The binding sensorgrams were fit to several models using CLAMP (version 99) (*29*). The five tested kinetic models include (1) a simple 1:1 Langmuir binding model, (2) a surface heterogeneity model, (3) a mass transfer limit model, (4) a simple conformation change model, and (5) a three-step reaction with an intermediate specie as described in Scheme 1. Fitting both the binding and dissociation phases of the sensorgram with the 1:1 Langmuir binding model yielded a poor fit as judged by the nonrandomness of residuals for both association and dissociation phases (Figure 6A). Further tests with a surface heterogeneity model, mass transfer limit model, and simple conformation change model likewise did not provide adequate fitting of the sensorgram (data not shown).

However, the three-step reaction model (Scheme 1) was capable of providing a superior fit of the binding data. This model describes three reaction steps where in the first step, gp44/62 (E) binds to the P−T DNA substrate (D) to give ED, which is converted to ED* that dissociates directly to E and D in an irreversible step. In this model, we assume that the previously observed slow steady-state ATP hydrolysis rate of 0.024 $s^{-1}$ (*30*) is most likely limited by the dissociation of the gp44/62−DNA intermediate (ED*) formed as the result of ATP hydrolysis. Therefore, we assigned a value of 0.024 $s^{-1}$ to the rate constant for dissociation of ED* to E and D. The dissociation step from ED* to E and D was also assumed to be irreversible since gp44/62 bound with ADP does not bind DNA (*vide ante*). Likewise, we argue that the ED to ED* step is biased to ED* on the basis of the lack of an observable positional isotope exchange (*19*).

As noted previously, this model provides a significant improvement in fitting versus other models. However, the rate constant for association of E and D to form ED is ~20-fold lower than the minimal association rate constant extracted from the rapid quench experiment (>8 × $10^6$ $M^{-1}$ $s^{-1}$) (*vide infra*). By including a mass transfer effect with the three-step model and setting $k_1$ equal to 8 × $10^6$ $M^{-1}$ $s^{-1}$, we achieved a satisfactory fit (Figure 6B). The goodness of fit is not affected by increasing the $k_1$ provided the ratio of $k_1/k_{-1}$ is maintained. Therefore, the resulting rate constants ($k_1$ and $k_{-1}$) represent lower limits.

A global fit of the DNA binding data obtained at different clamp loader concentrations allowed us to estimate the kinetic rate constants summarized in Table 3. Note that fitted rate constant $k_2$ (ca. 0.9 $s^{-1}$) most likely represents a step after the ATP hydrolysis because results of the rapid quench experiment in which gp44/62 and DNA are rapidly mixed with ATP indicate the chemical step of ATP hydrolysis should occur with a rate constant of >20 $s^{-1}$. We speculate that a conformational change accompanying ADP/$P_i$ release

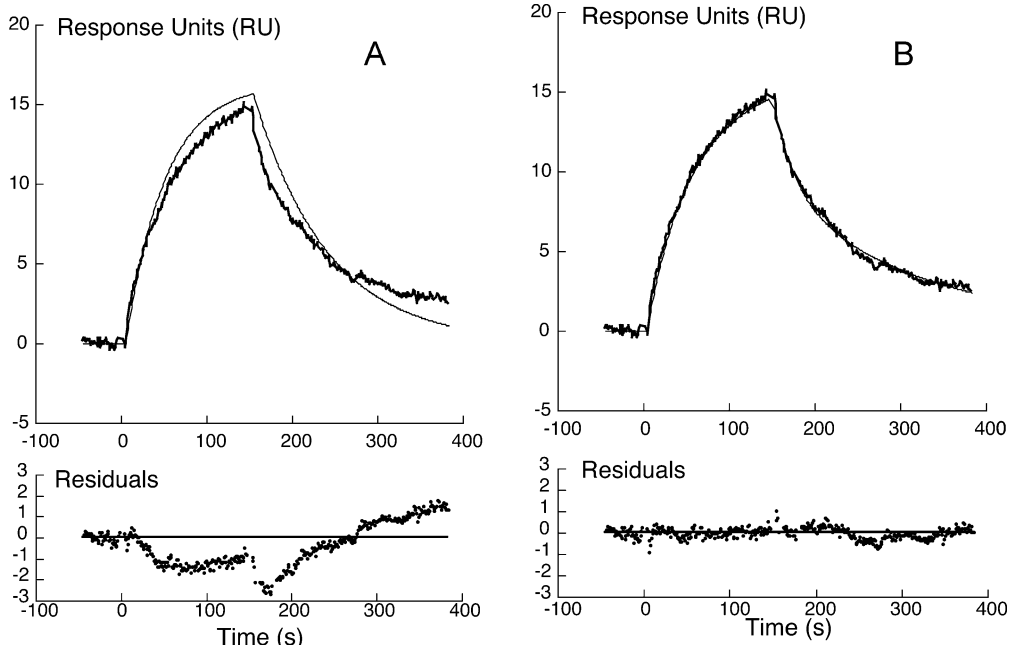


FIGURE 6: Representative sensorgram of binding of 200 nM gp44/62 to P−T DNA in the presence of 1 mM ATP fitted to either (A) a simple Langmuir model or (B) the three-step binding model as described in Scheme 1. The fitted line and the residuals showing the goodness of fit are also shown.

Table 3: Kinetic Data for Binding of gp44/62 to P−T DNA Derived from SPR Biosensor Measurements

| $k_1$ ($M^{-1}$ $s^{-1}$) | $k_{-1}$ ($s^{-1}$) | $k_2$ ($s^{-1}$) | $k_{-2}$ ($M^{-1}$ $s^{-1}$) | $k_3$ ($s^{-1}$) |
|---|---|---|---|---|
| $8 \times 10^6$ | 4.5 | 0.9 | $8 \times 10^4$ | 0.024 |

could be involved in this step. Two conclusions can be drawn. (1) gp44/62 binds to DNA with only moderate affinity in the initial binding step as judged from the equilibrium binding constant of ca. 500 nM for the gp44/62−DNA complex (ED). (2) The gp44/62−DNA intermediate specie (ED*) has enhanced binding affinity reflected in a ca. 200-fold reduction in the dissociation rate constants ($k_{-1}$ vs $k_3$).

*The gp44/62−DNA (ED*) Complex Is Active in Clamp Loading.* Having demonstrated that gp44/62 can form a complex with DNA, we next tested whether this complex can actively load the clamp. Previous studies have focused on a clamp loading model that first invokes formation of the gp44/62−gp45 complex with the consumption of 2 equiv of ATPs followed by the loading of the clamp upon the interaction of this complex with P−T DNA (*7*). Alternatively, the active holoenzyme could also be effectively assembled when a preformed gp44/62−DNA−ATP complex was rapidly mixed with gp45 and gp43 (*31*), suggesting that a gp44/62−DNA complex might also suffice.

To test this hypothesis, the transient clamp subunit interface distances were measured when the clamp was mixed with the preformed gp44/62−DNA complex using stopped-flow fluorescence spectroscopy. The gp44/62−DNA complex was formed in syringe A containing 1 $\mu$M gp44/62, 1 $\mu$M DNA [the forked Bio62/34/36 primer−template blocked with streptavidin as described previously (*15*)], and 2 mM ATP. Because of the low level of steady-state ATPase activity of gp44/62 in the presence of DNA ($k_{cat} = 0.024$ $s^{-1}$), this excess ATP is sufficient during the course of the experiment to prevent significant nucleotide depletion. The gp44/62−DNA complex formed in syringe A was rapidly mixed with 1 $\mu$M V163C/W199F-CPM or W92F/V163C/W199F-CPM in syringe B in two parallel experiments. When V163C/W199F-CPM was excited at 290 nm and the CPM fluorescence was detected by using a 420 nm cutoff filter, two processes were observed: a fast increase in CPM fluorescence followed by a slower phase (Figure 7). Repeating this experiment with W92F/V163C/W199F-CPM excited at both 290 and 390 nm yielded two similar increases in CPM fluorescence (data not shown).

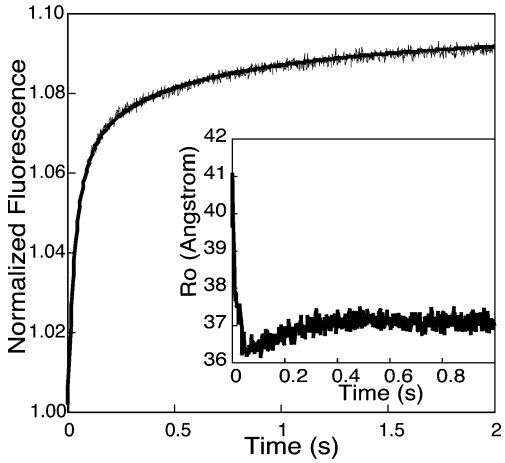


FIGURE 7: Normalized stopped-flow fluorescence values for mixing of gp44/62, DNA, and ATP with gp45 V163C/W199F-CPM. The solid line represents a KinTekSim simulation using steps 6−9 as described in Scheme 2. The calculated gp45 open interface distance (angstroms) changing as a function of time is shown in the inset.

On the basis of the time course of normalized fluorescence $F_{AD}^{290}$ (V163C/W199F-CPM excited at 290 nm), $F_A^{290}$ (W92F/V163C/W199F-CPM excited at 290 nm), and $F_A^{390}$ (W92F/V163C/W199F-CPM excited at 390 nm), the time-dependent changes in $I_{AD}$ and $I_A$ were calculated as described in Materials and Methods. The intramolecular FRET efficiency ($E_T$) between Trp92 and V163C-CPM can be calculated using eq 3, and its changes with time can be traced.

With the assumption that two of the three gp45 subunits are closed with an energy transfer efficiency ($E_C$) of 0.95, the open interface energy transfer efficiency ($E_O$) can be related to the total energy transfer efficiency ($E_T$) by eq 5 (*6*), and subsequently to the W92−V163C-CPM separation distance in the open gp45 interface. The resulting time-dependent change in open interface distance $R_O$ is shown in the inset of Figure 7.

When the gp44/62−DNA complex was mixed with gp45, a rapid decrease in the open interface distance from 41 to ~36 Å was completed within 50 ms. In a second phase, the subunit distance slightly increases and reaches a final plateau of 37 Å. This result suggests an immediate closing of the gp45 clamp (with its open subunit interface of 40 Å) around the DNA when the gp44/62−DNA complex is mixed with gp45. There is no further opening of the clamp as observed before upon formation of the gp44/62−gp45 complex (*6*). The distance of 37 Å is close to the value of 35 Å previously observed for the gp45−gp44/62−DNA complex generated by adding the gp44/62−gp45 complex to DNA (*6*). Although loaded through two different pathways, gp45 apparently adopts a similar conformation once bound to DNA. We also observed a slight increase in the interface distance in the second phase, possibly due to an out-of-plane conformational change followed by an in-plane closing of the clamp as previously proposed (*32*).

*Pre-Steady-State ATP Hydrolysis Measurements.* Transient kinetic experiments were performed using a rapid-quench instrument as described previously (*7*) to define the stoichiometries and rate constants of ATP hydrolysis by gp44/62 for the different loading pathways. Four distinct experiments were performed in which gp44/62 was preincubated in differing combinations with the various components used in the clamp loading process. As a control, we assessed ATP consumption by mixing a preincubated solution of the gp44/62−DNA−gp45 complex with ATP and observed a burst amplitude of 7.5 ± 1.0 $\mu$M that corresponds to a stoichiometry of 4 equiv of ATP consumed per clamp loading event, consistent with an earlier finding (*7*). Second, we assessed ATP consumption under conditions in which a preincubated gp44/62/DNA mixture was mixed with gp45 and ATP. The time course of ATP hydrolysis was identical to that in the aforementioned experiment with a burst of 4 equiv of ATP hydrolyzed, suggesting a similar equilibration of reaction species independent of mixing. Third, we investigated the extent of ATP hydrolysis when ATP alone was added to a solution of gp44/62 and DNA. Over the time frame that was examined (0.01−5 s), the generated time course in ATP consumption is best fit to a single-exponential curve followed by a steady-state turnover (Figure 8). The burst amplitude is 2.0 ± 0.3 $\mu$M, which corresponds to a stoichiometry of 1 equiv of ATP consumed at a rate of 19.7 ± 7.0 $s^{-1}$ during the interaction of the clamp loader with P−T DNA to form the ED* complex (Scheme 1).

Finally, we performed analogous transient experiments to measure the amount of ATP consumed by the DNA-bound gp44/62 (ED* complex) upon interacting with the clamp protein. In these experiments, gp44/62 was preincubated with DNA and ATP and then mixed with gp45. This is a technically challenging experiment since gp44/62 will hydrolyze an appreciable amount of ATP during the preincubation process due to the presence of DNA. To clearly define the amount of ATP consumed during clamp loading, the "background" amount of ATP hydrolysis must be subtracted from each corresponding time point obtained from the rapid quench experiment. To accomplish this, we performed a separate experiment in parallel by monitoring the amount of ATP consumed by gp44/62 in the presence of only DNA. No burst phase of ATP hydrolysis was noted during the time course, and a ATP hydrolysis rate of 0.72 $s^{-1}$ was observed (data not shown).

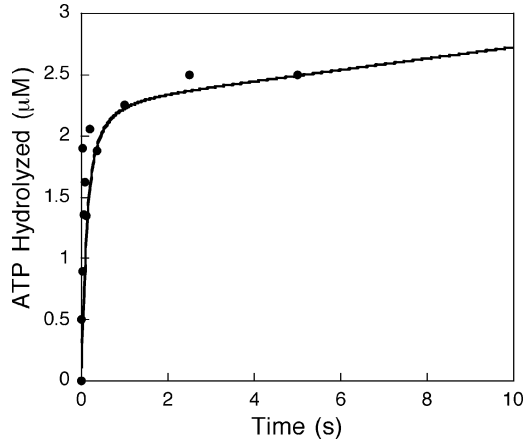


FIGURE 8: Pre-steady-state ATP hydrolysis during the reaction of mixing gp44/62, DNA and ATP. The time course reveals a burst amplitude of 1 equiv of ATP followed by a slow steady-state ATP hydrolysis rate. The solid line represents a KinTekSim simulation using steps 1−5 as described in Scheme 2. A factor of 1.2 was used in the simulation to correct for the possible error in protein/ATP concentration.

## DISCUSSION

*Binding of MANT-ATP to gp44/62 Induces a Conformational Change.* T4 clamp loader gp44/62 belongs to the versatile AAA+ protein family (ATPases associated with a variety of cellular activities). AAA+ proteins are involved in a myriad of biological processes, including ATP-dependent proteolysis, membrane fusion, protein trafficking, and DNA replication, recombination, and repair. Despite the diverse functions, all are driven by ATP binding and hydrolysis. The AAA+ protein subunit normally consists of three domains, and two of them (domains I and II) are highly conserved and form well-defined amino acid sequence motifs. Domain I is an anchor domain that together with domain II constitutes the ATP binding and hydrolysis site, which are characterized by Walker A and B motifs and sensor 1 and 2 motifs. Domain III is highly variable among different AAA+ proteins and is responsible for the interaction with specific protein or DNA targets. Domain III retains considerable conformational freedom relative to the other two domains. Therefore, possible conformation changes in domains I and II induced by ATP binding and hydrolysis can be transmitted to domain III, which would in turn be translated into specific molecular functions.

gp44/62 is a tightly associated complex consisting of four gp44 subunits and one gp62 subunit. The gp44 subunits contain the ATP binding and hydrolysis domains (*26*), while the gp62 subunit is required for interaction with clamp gp45 (*18*). Although a high-resolution X-ray crystal structure of gp44/62 is not available, the gp44 subunit shares considerable amino acid sequence similarities with the other clamp

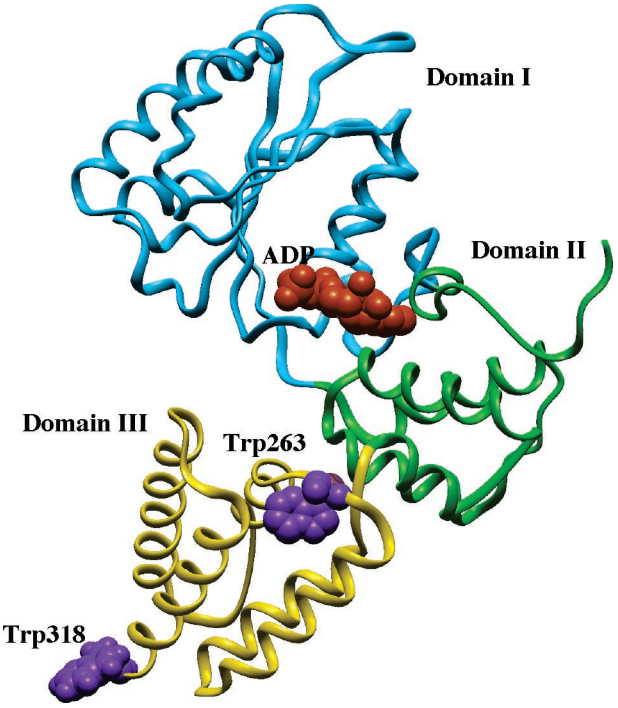


FIGURE 9: Ribbon representation of the modeled three-dimensional structure of the gp44 subunit with ADP bound (red). Domain I and domain II that form the ATP-binding site are colored cyan and green, respectively. Domain III is colored yellow. The two tryptophan residues (Trp263 and Trp318) located in domain III are shown as a CPK model (purple).

loaders, including the small subunit of the RFC complex from *Pyrococcus furiosus* (24% sequence identity). The archaeal clamp loader RFC complex from *P. furiosus* consists of one large subunit (RFCL, 55 kDa) and four small subunits (RFCS, 37 kDa). In the determined *P. furiosus* RFC small subunit structure, domain I and domain II form the canonical nucleotide binding cleft and bind ADP. By using the threading program 3D-PSSM (*33*), a modeled three-dimensional structure of gp44 (Figure 9) was generated with a high degree of confidence (*E* value of $1.84 \times 10^{-12}$) using the *P. furiosus* RFCS X-ray crystal structure as a template. A pairwise sequence alignment between the two proteins reveals that the T4 gp44 contains the highly similar Walker A and Walker B motifs and sensor 1 and sensor 2 motifs that are found in *P. furiosus* RFCS. On the basis of the primary structure and fold similarity, it is evident that a similar nucleotide binding site is expected for T4 gp44, which allows the nucleotide ADP to be modeled into the gp44 structure (Figure 9).

The T4 gp44 subunit amino acid sequence contains two tryptophan residues, namely, Trp263 and Trp318, which reside in domain III of T4 gp44. From the modeled gp44−ADP complex structure, the distance between bound ADP and Trp263 is 27 Å, compared to a distance of ~50 Å between ADP and Trp318. The former distance is close to the $R_0$ (~20 Å) for the Trp−MANT FRET pair, while the latter is much larger than $R_0$. Therefore, the FRET signal detected in both the steady-state and stopped-flow FRET experiments with the MANT-nucleotide is likely derived from the Trp263 and MANT-nucleotide fluorophore. Although the gp62 subunit contains several Trp residues, the distances between the MANT-nucleotide and the gp62 Trps are probably beyond the detectable range and therefore do not contribute to the observed FRET signal. This hypothesis is partially supported by the observation that the similar two-phase stopped-flow trace was observed for the gp44 subunit alone, as compared to that of the complete gp44/62 complex.

The first phase of rapid mixing MANT-ATP with gp44/62 is apparently due to nucleotide binding. The values of $k_{1,obs}$ are proportional to the MANT-ATP concentration used. A phase for nucleotide binding is also evident when MANT-ADP is mixed with gp44/62. The kinetic rate constants determined for MANT-ADP are not very different from those determined for MANT-ATP. These results suggest that the gp44/62 nucleotide binding site has a similar affinity for either nucleotide. However, in the transients of binding of MANT-ATP to gp44/62, a second slower phase is evident, while a similar phase is absent in the MANT-ADP binding transients. Given the intrinsic ATPase activity of gp44/62, we first considered whether the slow phase is due to the hydrolysis of MANT-ATP following the binding step. The rate constant for ATP hydrolysis catalyzed by gp44/62 alone is $<0.012\ s^{-1}$ (*30*) and ~1000-fold lower than the observed $k_2$. Furthermore, the rate constant of $\sim 0.012\ s^{-1}$ cannot reflect product release since MANT-ADP dissociation is ~7500 times faster ($k_{off} = 89\ s^{-1}$). Therefore, the slow rate likely reflects a kinetic step preceding hydrolysis. Consequently, we propose that the second phase in the transient is most likely due to a conformational change in gp44/62 induced by the binding of MANT-ATP. A similar conformational change step fellowing ATP binding has been documented for the *E. coli* $\gamma$ complex with a rate constant of $6.5\ s^{-1}$ (*34*). We conclude that only ATP binding triggers such a specific conformational change in the T4 clamp loader, while ADP binding is ineffective. We can speculate about the molecular nature of the observed conformation change based on the modeled gp44/62−nucleotide structure. Since the FRET donor, Trp263, is located in domain III of the gp44 subunit, while the MANT-ATP binding site is formed by domains I and II, it is most likely that MANT-ATP binding brings domain III closer to domains I and II, thus resulting in an increase in the level of fluorescence energy transfer.

The binding of MANT-ATP to gp44 showed kinetic and equilibrium constants similar to those of gp44/62 (see Table 2). Therefore, the absence of the gp62 subunit seemingly has no impact on binding of nucleotide to the gp44 subunit. On the basis of the biochemical and structural studies of *E. coli* and yeast clamp loaders, the ATPase active site of the clamp loader is formed by two neighboring subunits that contribute either the conserved ATP binding motifs or the arginine finger required for ATP hydrolysis. Since the gp62 sequence contains neither component, it is likely that gp62 does not participate in the formation of the ATPase site such that its removal results in no obvious effect in ATP binding.

*DNA Binding Activity of gp44/62.* Through multiple-sequence alignment of the T4 gp44 subunit and the five RFC subunits of the yeast clamp loader and the $\gamma$ subunit of the *E. coli* $\gamma$ complex, we found that the gp44 subunit possesses not only the important ATPase site residues but also several conserved residues (Lys80, Arg85, and Arg119) that have been implicated in DNA binding (*35*). These observations suggest that gp44/62 possesses an intrinsic DNA binding ability.

We then demonstrated that gp44/62 has an intrinsic affinity for P−T DNA with a recessed 3′-end. This specific binding

required ATP because gp44/62 alone exhibited negligible binding to P−T DNA. The role played by ATP in binding cannot be filled by ADP and ATP$\gamma$S. Furthermore, the DNA binding affinity of gp44/62 is also dependent upon DNA structure. It does not bind to single-stranded DNA and binds only weakly to duplex DNA with a blunt end. These observations distinguish gp44/62 from other clamp loaders, such as the yeast RFC complex and the *E. coli* $\gamma$ complex, in terms of DNA binding. The yeast RFC complex binds to P−T DNA only when ATP$\gamma$S is present and ATP is not effective in supporting DNA binding (*36*). The *E. coli* $\gamma$ complex binds strongly to P−T DNA in the presence of ATP$\gamma$S but only weakly in the presence of ATP (*37*). In addition, the *E. coli* $\gamma$ complex can also bind single-stranded DNA in the presence of ATP (*37*).

The observation that hydrolytically inert ATP analogue such as ATP$\gamma$S does not support binding of gp44/62 to P−T DNA suggests that the DNA binding event must involve ATP hydrolysis. This again contrasts with data obtained for yeast and *E. coli* clamp loaders in which ATP hydrolysis decreases the affinity of the clamp loader for DNA. The hydrolysis of ATP is likely required for "locking" gp44/62 into an effective P−T DNA binding conformation. In support of our observation, we found that mutant clamp loader gp44(K56A)/62 was unable to bind P−T DNA even in the presence of ATP. Consequently, both binding and hydrolysis of ATP are required for binding of the T4 clamp loader to DNA.

The SPR binding data allowed us to construct a minimal pathway for the DNA binding and ATP hydrolysis pathway for gp44/62. In general, binding of gp44/62 to P−T DNA cannot be described by a simple Langmuir model. Since P−T DNA effectively triggers ATP hydrolysis and presumably converts gp44/62 into a different conformational state, we tested a three-step model (Scheme 1). The fit was generally satisfactory for both binding and dissociation phases. We conclude that the initial complex formed between gp44/62 and DNA (ED) is converted to a more stable complex (ED*) presumably as the result of ATP hydrolysis.

*gp44/62 in Complex with P−T DNA Loads the Clamp Protein.* Previous steady-state and time-resolved FRET studies unambiguously demonstrated that the T4 clamp exists as an open form in solution. The functional significance of this unique clamp structure has remained unclear. An earlier study showed that by inclusion of a crowding reagent, PEG, in the reaction solution, the T4 clamp gp45 can effectively form the active holoenzyme with gp43 on a singly primed single-stranded circular M13 DNA in the absence of gp44/62 (*38*). The nonenzymatic loading of the clamp with the help of a crowding reagent is consistent with our present understanding that the clamp is already open in solution. Therefore, a possible role for gp44/62 in the clamp loader−DNA complex could be to guide the opened clamp protein onto the 3′-end of P−T DNA in an orientation for productive binding with the incoming polymerase. We utilized stopped-flow FRET to follow the transient clamp interface distance changes accompanying clamp loading and found the combination of the clamp protein with the gp44/62−DNA complex resulted in a rapid decrease in the open clamp subunit interface distance from 41 to ~36 Å, indicative of the closing of the clamp onto DNA. The lack of an initial phase reflecting clamp opening suggests that further opening of the clamp is unnecessary for clamp loading in this loading sequence and differs from our observation in a previously described loading pathway that features an initial gp44/62−gp45 complex (*6*).

*Utilization of ATP by gp44/62 in the Current Clamp Loading Pathway.* Given a clamp with an open interface distance that is sufficiently large to allow the passage of double-stranded DNA, it is puzzling that gp44/62 appears to hydrolyze 2 equiv of ATP upon interacting with gp45 to open the clamp further. To study the utilization of ATP by gp44/62 for the current loading pathway, we assessed the pre-steady-state ATP hydrolysis by gp44/62 under different preincubation conditions. The alternative pathway for clamp loading uses only 1 equiv of ATP to form the clamp loader−DNA complex and to reorganize gp44/62 into a productive conformation for subsequent loading of the clamp. When gp44/62 was preincubated with DNA in the presence of ATP and then mixed with gp45, only a single linear phase of ATP hydrolysis was observed. We interpret this result by proposing that closing of the clamp onto DNA in the current pathway may not require ATP hydrolysis. The ATP hydrolysis event observed in the steady-state phase is likely required for dissociation of the clamp loader from its complex with the clamp and DNA in the absence of gp43. At present, we cannot unequivocally determine the total number of equivalents of ATP hydrolyzed in a given step in the above-mentioned process due to the lack of biphasic ATP hydrolysis.

*Kinetic Simulation of Experimental FRET and Pre-Steady-State ATPase Data.* On the basis of the available information regarding the alternative clamp loading pathway, we propose a minimal kinetic scheme as depicted in Scheme 2. The stopped-flow FRET traces for MANT-nucleotide binding and the rapid quench ATPase data in combination with the SPR binding data were used to derive the respective rate constants in steps 1−5. For step 1, the rate constants for binding of ATP to gp44/62 were determined from the stopped-flow FRET experiments with the MANT analogue. For the sake of simplicity, we have not included the conformational change step noted earlier. The rapid quench ATPase data for mixing gp44/62, DNA, and ATP were used to derive the rate constants for steps 2, 3, and 5 by data simulation using KinTekSim, and the rate constant for step 4 was imported directly from the SPR study presuming it is due to ADP/$P_i$ release. Note that the rate constants in step 2 represent a lower limit of the true values. Figure 8 shows simulation of the rapid quench ATPase data using steps 1−5. Steps 6−9 represent the loading of the clamp onto DNA by the preformed gp44/62−DNA complex. The stopped-flow trace in Figure 7 was simulated using steps 6−9. The rate constants were individually varied to determine the best fit to the data, and the ranges of rate constants that provide a satisfactory simulation of the data are presented in Scheme 2. Steps 10 and 11 describe the last stage of holoenzyme formation via introduction of gp43. Previous experiments have shown that by preincubating gp44/62 with DNA in the presence of ATP and then simultaneously introducing gp43 and gp45 one can form the holoenzyme at a rate of 1.3 $s^{-1}$ (*31*). This rate constant is in good agreement with the simulated rate constant for step 8 (1.5−2 $s^{-1}$), which is the slowest step between steps 6 and 8. The binding of gp43 to the tertiary complex (gp44/62−DNA−gp45) is fast (*7*) and should not be a rate-limiting step. It is currently established

Scheme 2: Clamp Loading and Holoenzyme Assembly Process Depicting the Current Clamp Loading Pathway with Initial Formation of the gp44/62−DNA Complex[a]

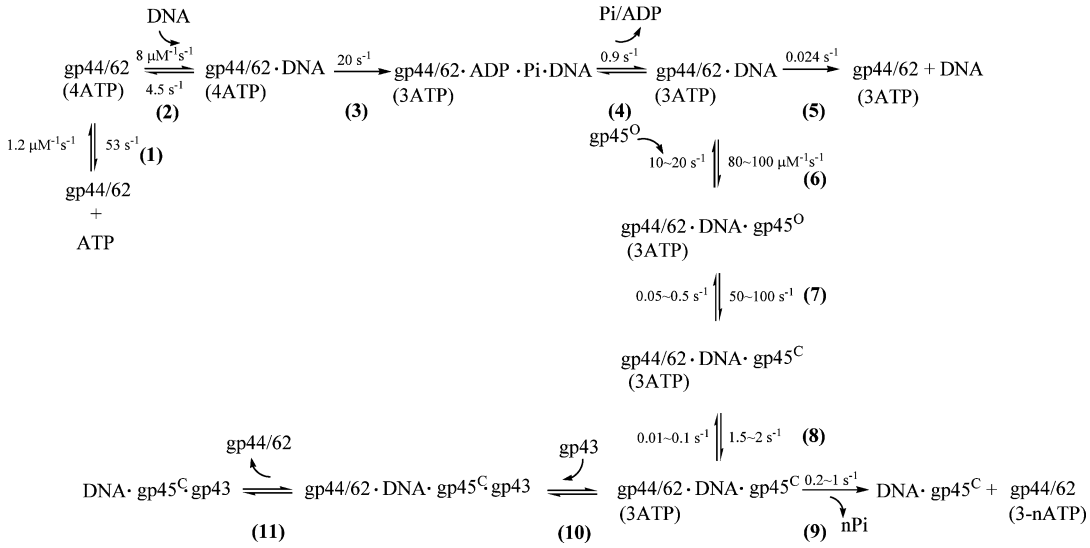


[a] The microscopic rate constants for step 1 were derived from pre-steady-state MANT-ATP binding experiments. The rate constants for steps 2−5 were obtained from both the pre-steady-state ATP hydrolysis and SPR binding experiments. Note the association rate constant of step 2 represents the minimal rate required for a sufficient fitting of the data. Rate constants for steps 6−9 were obtained by simulating the stopped-flow data for the mixing of the gp44/62−DNA complex with gp45. The range of rate constants that provides a sufficient fitting is presented.

that 1 equiv of ATP is hydrolyzed in step 3 in the assembly pathway. Our rapid quench experiment in which the gp44/62−DNA−ATP complex is mixed with gp45 showed no burst of ATP hydrolysis. This observation suggests that the clamp loading process as described in steps 6−8 involves no ATP hydrolysis. Instead, the electrostatic interaction between the negatively charged DNA backbone and positively charged residues in the inner surface of gp45 may effectively drive this clamp closing process. We tentatively assign the ATP hydrolysis event to step 9 on the basis of the fact that the rate of this step derived from simulation of the stopped-flow FRET data for mixing the gp44/62−DNA−ATP complex with gp45 is in good agreement with the ATP hydrolysis rate constant of 0.72 $s^{-1}$ determined by rapid quench experiments. Because of the lack of biphasic kinetics for ATP hydrolysis, we have not been able to determine the actual number of equivalents of ATP hydrolyzed in step 9.

*Clamp Loading Compared.* Studies on the *E. coli* $\gamma$ complex show that upon ATP binding, the $\gamma$ complex is converted to an "active" DNA binding state with a high affinity for P−T DNA. However, once the complex is bound to DNA, a fast ATP hydrolysis step converts the $\gamma$ complex to an "inactive state" with a greatly reduced affinity for DNA (the $K_d$ changes from 2 nM to 6 $\mu$M) (*37*). The rate for dissociation of the $\gamma$ complex from DNA is fast (85 $s^{-1}$). Consequently, this pathway is not desirable for loading the clamp. Alternatively, the interaction of the $\gamma$ complex with the $\beta$ clamp in the presence of ATP provides a stable ternary complex with no consumption of ATP. This complex in turn binds to DNA and loads the clamp. The ensuing hydrolysis of 2 equiv of ATP weakens the association of the $\gamma$ complex with $\beta$, leading to dissociation of the $\gamma$ complex from DNA.

The binding of yeast clamp loader RFC to P−T DNA is also dependent on ATP binding, and likewise, ATP hydrolysis actively dissociates RFC from DNA (*36*). Thus, RFC is similar to the *E. coli* $\gamma$ complex in terms of intrinsic DNA binding ability, and the sequence of clamp loading events suggests that proper PCNA loading requires RFC to bind PCNA prior to binding to DNA (*36*).

The experimental results presented in this study clearly indicate that the T4 gp44/62 clamp loader is markedly different from its *E. coli* and yeast counterparts. First, a relatively stable gp44/62−DNA complex is readily formed as the result of ATP binding and hydrolysis. Second, this gp44/62−DNA binary complex is active in loading gp45 onto DNA. A third distinction is the differences in the timing of ATP hydrolysis events in driving the required conformational changes needed for clamp loading. The clamp loaders from all three different organisms possess intrinsic ATP binding and hydrolysis activity. In each case, the ATPase activities of the clamp loader alone are minimal but synergistically stimulated by the presence of both the clamp and DNA. However, depending on the identity of the clamp loader, the ATPase activities are modulated differently by the clamp and DNA.

In the case of the *E. coli* $\gamma$ complex, the interaction with the $\beta$ clamp suppresses its steady-state ATPase activity by 6-fold, presumably due to the formation of a stable ATP-bound $\gamma$ complex−$\beta$ specie (*8*). In contrast to the $\beta$ clamp, DNA can effectively stimulate the ATPase activity of the $\gamma$ complex. When the $\gamma$ complex is mixed with DNA and ATP in the absence of $\beta$ clamp, 2 equiv of ATP is rapidly consumed followed by a steady-state phase with an ATP hydrolysis rate 20-fold higher than the rate obtained with $\beta$. Collectively, these results are in accord with the formation of a transient $\gamma$−DNA complex that is dissociated by rapid ATP hydrolysis. The steady-state ATPase activities of yeast RFC, which parallel those observed for the *E. coli* $\gamma$ complex, are likewise stimulated to a lesser extent by its cognate clamp, PCNA, but more by DNA (*36*).

As opposed to its *E. coli* and yeast counterparts, gp44/62 ATPase activity is stimulated greatly by gp45 (20-fold increase in $k_{cat}$) as compared to a merely 2-fold stimulation by P−T DNA (*19*). The observation that a burst of ATP

hydrolysis was observed when gp44/62 is rapidly mixed with DNA clearly indicates a slow step after ATP hydrolysis sets the limit for steady-state turnover. The most likely kinetic steps would be dissociation of the binary complex or the subsequent cycling of gp44/62 back from a possible inactive DNA-binding state to an active state as proposed for the interaction of the *E. coli* $\gamma$ complex with DNA (*37*). Since such an inactive state has not yet been detected for gp44/62, a slow dissociation of gp44/62 from DNA is most likely the rate-limiting step.

The functional distinction of T4 clamp loading is also related to the unique solution structure of gp45. Instead of a closed ring as observed for $\beta$ and PCNA, T4 gp45 exists as an opened ring in solution. In both *E. coli* and yeast *S. cerevisiae*, the formation of a binary complex of the clamp loader and DNA leads to hydrolysis of bound ATP and, hence, the rapid dissociation of the clamp loader from DNA. Although energetically inefficient, this process is physiologically important because a stable clamp loader−DNA complex may present a topological problem for loading a closed clamp.

This notion is self-evident in viewing the recently determined structure of the yeast RFC−PCNA complex (*39*). In the complex structure, the five ATPase subunits of the RFC complex adapt a spiral configuration and form an inner chamber that presumably accommodates duplex DNA. Three of the five ATPase subunits make contact with the PCNA ring. It is clear from this structure that the initial formation of the RFC−DNA binary complex will make it topologically difficult to form a productive interaction with PCNA, thus hindering the clamp opening. However, this may not present a problem for T4 since an opened clamp can readily encircle duplex DNA and establish interactions with the gp44/62 simultaneously. Therefore, we speculate that the current clamp loading pathway, unique to the T4 clamp loading system compared to the other two model systems (*E. coli* and *S. cerevisiae*), may have co-evolved with T4 gp45 that exists as an open instead of closed ring in solution.

## CONCLUSION

In this work, we demonstrated that gp44/62 is able to load the gp45 clamp protein onto DNA through the initial formation of a gp44/62−DNA complex. In this model, the binding of ATP to gp44/62 induces a conformational change in gp44/62 that configures the clamp loader for effective DNA binding. A gp44/62−DNA complex is formed with the hydrolysis of 1 equiv of ATP to interact with the opened form of gp45 on P−T DNA and orient the clamp properly through interaction between the specific clamp face and clamp loader. No ATP consumption is required for the formation of the ternary complex. The closing of the clamp may be driven by the electrostatic interaction between the clamp and DNA. This pathway differs from the previously demonstrated clamp loading pathway in which a gp44/62−gp45 complex interacts with DNA to load the clamp. Thus, the bacteriophage T4 clamp loading pathway can proceed via a random mechanism that may reflect physiological conditions depending on the replisome organization. These include the spatial arrangement between the protein components and DNA, the specific protein interactions between the holoenzyme accessory proteins, and other replisome components such as single-stranded DNA binding protein and primosome proteins.

## ACKNOWLEDGMENT

We thank Dr. Michelle M. Spiering for material and helpful discussion.

## SUPPORTING INFORMATION AVAILABLE

Binding of MANT-ATP to the gp44 subunit followed by stopped-flow FRET (Figure 1), a SPR sensorgram of binding of gp44/62 to P−T DNA in the presence of ATP, ATP$\gamma$S, or an equimolar mixture of ATP and ATP$\gamma$S (Figure 2), and a SPR sensorgram of binding of gp44(K56A)/62 to P−T DNA (Figure 3). This material is available free of charge via the Internet at http://pubs.acs.org.

## REFERENCES

1. Benkovic, S. J., Valentine, A. M., and Salinas, F. (2001) Replisome-mediated DNA replication, *Annu. Rev. Biochem. 70*, 181−208.
2. Baker, T. A., and Bell, S. P. (1998) Polymerases and the replisome: Machines within machines, *Cell 92*, 295−305.
3. Mace, D. C., and Alberts, B. M. (1984) T4 DNA polymerase rates and processivity on single-stranded DNA templates, *J. Mol. Biol. 177*, 295−311.
4. Johnson, A., and O'Donnell, M. (2005) Cellular DNA replicases: Components and dynamics at the replication fork, *Annu. Rev. Biochem. 74*, 283−315.
5. Berdis, A. J., Soumillion, P., and Benkovic, S. J. (1996) The carboxyl terminus of the bacteriophage T4 DNA polymerase is required for holoenzyme complex formation, *Proc. Natl. Acad. Sci. U.S.A. 93*, 12822−12827.
6. Alley, S. C., Abel-Santos, E., and Benkovic, S. J. (2000) Tracking sliding clamp opening and closing during bacteriophage T4 DNA polymerase holoenzyme assembly, *Biochemistry 39*, 3076−3090.
7. Trakselis, M. A., Berdis, A. J., and Benkovic, S. J. (2003) Examination of the role of the clamp-loader and ATP hydrolysis in the formation of the bacteriophage T4 polymerase holoenzyme, *J. Mol. Biol. 326*, 435−451.
8. Hingorani, M. M., Bloom, L. B., Goodman, M. F., and O'Donnell, M. (1999) Division of labor: Sequential ATP hydrolysis drives assembly of a DNA polymerase sliding clamp around DNA, *EMBO J. 18*, 5131−5144.
9. Bertram, J. G., Bloom, L. B., Hingorani, M. M., Beechem, J. M., O'Donnell, M., and Goodman, M. F. (2000) Molecular mechanism and energetics of clamp assembly in *Escherichia coli*. The role of ATP hydrolysis when $\gamma$ complex loads $\beta$ on DNA, *J. Biol. Chem. 275*, 28413−28420.
10. Hingorani, M. M., and O'Donnell, M. (1998) ATP binding to the *Escherichia coli* clamp loader powers opening of the ring-shaped clamp of DNA polymerase III holoenzyme, *J. Biol. Chem. 273*, 24550−24563.
11. Alley, S. C., Shier, V. K., Abel-Santos, E., Sexton, D. J., Soumillion, P., and Benkovic, S. J. (1999) Sliding clamp of the bacteriophage T4 polymerase has open and closed subunit interfaces in solution, *Biochemistry 38*, 7696−7709.
12. Millar, D., Trakselis, M. A., and Benkovic, S. J. (2004) On the solution structure of the T4 sliding clamp (gp45), *Biochemistry 43*, 12723−12727.
13. Yao, N., Turner, J., Kelman, Z., Stukenberg, P. T., Dean, F., Shechter, D., Pan, Z. Q., Hurwitz, J., and O'Donnell, M. (1996) Clamp loading, unloading and intrinsic stability of the PCNA, $\beta$ and gp45 sliding clamps of human, *E. coli* and T4 replicases, *Genes Cells 1*, 101−113.
14. Moarefi, I., Jeruzalmi, D., Turner, J., O'Donnell, M., and Kuriyan, J. (2000) Crystal structure of the DNA polymerase processivity factor of T4 bacteriophage, *J. Mol. Biol. 296*, 1215−1223.
15. Kaboord, B. F., and Benkovic, S. J. (1995) Accessory proteins function as matchmakers in the assembly of the T4 DNA polymerase holoenzyme, *Curr. Biol. 5*, 149−157.
16. Frey, M. W., Nossal, N. G., Capson, T. L., and Benkovic, S. J. (1993) Construction and characterization of a bacteriophage T4

DNA polymerase deficient in 3′-to-5′ exonuclease activity, *Proc. Natl. Acad. Sci. U.S.A. 90*, 2579−2583.
17. Nossal, N. G. (1979) DNA replication with bacteriophage T4 proteins. Purification of the proteins encoded by T4 genes 41, 45, 44, and 62 using a complementation assay, *J. Biol. Chem. 254*, 6026−6031.
18. Rush, J., Lin, T. C., Quinones, M., Spicer, E. K., Douglas, I., Williams, K. R., and Konigsberg, W. H. (1989) The 44P subunit of the T4 DNA polymerase accessory protein complex catalyzes ATP hydrolysis, *J. Biol. Chem. 264*, 10943−10953.
19. Berdis, A. J., and Benkovic, S. J. (1997) Mechanism of bacteriophage T4 DNA holoenzyme assembly: The 44/62 protein acts as a molecular motor, *Biochemistry 36*, 2733−2743.
20. Jarvis, T. C., Newport, J. W., and von Hippel, P. H. (1991). Stimulation of the processivity of the DNA polymerase of bacteriophage T4 by the polymerase accessory proteins. The role of ATP hydrolysis, *J. Biol. Chem. 266*, 1830−1840.
21. Piperno, J. R., and Alberts, B. M. (1978). An ATP stimulation of T4 DNA polymerase mediated via T4 gene 44/62 and 45 proteins. The requirement for ATP hydrolysis, *J. Biol. Chem. 253*, 5174−5179.
22. Moore, K. J., and Lohman, T. M. (1994) Kinetic mechanism of adenine nucleotide binding to and hydrolysis by the *Escherichia coli* Rep monomer. 1. Use of fluorescent nucleotide analogues, *Biochemistry 33*, 14550−14564.
23. Woodward, S. K., Eccleston, J. F., and Geeves, M. A. (1991) Kinetics of the interaction of 2′(3′)-O-(*N*-methylanthraniloyl)-ATP with myosin subfragment 1 and actomyosin subfragment 1: Characterization of two acto-S1-ADP complexes, *Biochemistry 30*, 422−430.
24. Jan, A. Y., Johnson, E. F., Diamonti, A. J., Carraway, K. L., III, and Anderson, K. S. (2000) Insights into the HER-2 receptor tyrosine kinase mechanism and substrate specificity using a transient kinetic analysis, *Biochemistry 39*, 9786−9803.
25. Latham, G. J., Pietroni, P., Dong, F., Young, M. C., and von Hippel, P. H. (1996) Fluorescence monitoring of T4 polymerase holoenzyme accessory protein interactions during loading of the sliding clamp onto the template-primer junction, *J. Mol. Biol. 264*, 426−439.
26. Jarvis, T. C., Paul, L. S., and von Hippel, P. H. (1989) Structural and enzymatic studies of the T4 DNA replication system. I. Physical characterization of the polymerase accessory protein complex, *J. Biol. Chem. 264*, 12709−12716.
27. Trakselis, M. A., Roccasecca, R. M., Yang, J., Valentine, A. M., and Benkovic, S. J. (2003) Dissociative properties of the proteins within the bacteriophage T4 replisome, *J. Biol. Chem. 278*, 49839−49849.
28. Capson, T. L., Benkovic, S. J., and Nossal, N. G. (1991) Protein-DNA cross-linking demonstrates stepwise ATP-dependent assembly of T4 DNA polymerase and its accessory proteins on the primer-template, *Cell 65*, 249−258.
29. Myszka, D. G., and Morton, T. A. (1998) CLAMP: A biosensor kinetic data analysis program, *Trends Biochem. Sci. 23*, 149−150.
30. Berdis, A. J., and Benkovic, S. J. (1996) Role of adenosine 5′-triphosphate hydrolysis in the assembly of the bacteriophage T4 DNA replication holoenzyme complex, *Biochemistry 35*, 9253−9265.
31. Sexton, D. J., Kaboord, B. F., Berdis, A. J., Carver, T. E., and Benkovic, S. J. (1998) Dissecting the order of bacteriophage T4 DNA polymerase holoenzyme assembly, *Biochemistry 37*, 7749−7756.
32. Trakselis, M. A., Alley, S. C., Abel-Santos, E., and Benkovic, S. J. (2001) Creating a dynamic picture of the sliding clamp during T4 DNA polymerase holoenzyme assembly by using fluorescence resonance energy transfer, *Proc. Natl. Acad. Sci. U.S.A. 98*, 8368−8375.
33. Kelley, L. A., MacCallum, R. M. and Sternberg, M. J. E. (2000) Enhanced genome annotation using structural profiles in the program 3D-PSSM, *J. Mol. Biol. 299*, 501−522.
34. Williams, C. R., Snyder, A. K., Kuzmic, P., O'Donnell, M., and Bloom, L. B. (2004) Mechanism of loading the *Escherichia coli* DNA polymerase III sliding clamp: I. Two distinct activities for individual ATP sites in the $\gamma$ complex, *J. Biol. Chem. 279*, 4376−4385.
35. Goedken, E. R., Kazmirski, S. L., Bowman, G. D., O'Donnell, M., and Kuriyan, J. (2005) Mapping the interaction of DNA with the *Escherichia coli* DNA polymerase clamp loader complex, *Nat. Struct. Mol. Biol. 12*, 183−190.
36. Gomes, X. V., and Burgers, P. M. (2001) ATP utilization by yeast replication factor C. I. ATP-mediated interaction with DNA and with proliferating cell nuclear antigen, *J. Biol. Chem. 276*, 34768−34775.
37. Ason, B., Bertram, J. G., Hingorani, M. M., Beechem, J. M., O'Donnell, M., Goodman, M. F., and Bloom, L. B. (2000) A model for *Escherichia coli* DNA polymerase III holoenzyme assembly at primer/template ends. DNA triggers a change in binding specificity of the gamma complex clamp loader, *J. Biol. Chem. 275*, 3006−3015.
38. Reddy, M. K., Weitzel, S. E., and von Hippel, P. H. (1993) Assembly of a functional replication complex without ATP hydrolysis: A direct interaction of bacteriophage T4 gp45 with T4 DNA polymerase, *Proc. Natl. Acad. Sci. U.S.A. 90*, 3211−3215.
39. Bowman, G. D., O'Donnell, M., and Kuriyan, J. (2004) Structural analysis of a eukaryotic sliding DNA clamp-clamp loader complex, *Nature 429*, 724−730.

BI0601205